COBEM 2023 27TH INTERNATIONAL CONGRESS OF MECHANICAL ENGENEERING

ABCM Brazilian Society of Mechanical Sciences and Engineering
27th ABCM International Congress of Mechanical Engineering
December 04-08, 2023, Florianópolis-SC, Brazil

COB-2023-1993
CONTROLLING THE RELAXATION AND BREAKUP OF INITIALLY ELONGATED FERROFLUID DROPLETS WITH ROTATING MAGNETIC FIELDS

Arthur L. Guilherme
Taygoara F. de Oliveira
Department of Mechanical Engineering, Energy and Environment Laboratory, 65070910. Brasília, DF, Brazil
tucaguilherme@gmail.com, taygoara@unb.br

Abstract. *The relaxation and breakup of an elongated superparamagnetic ferrofluid droplet immersed in a nonmagnetic viscous fluid subjected to static and rotating uniform magnetic fields are considered by using a multiphase numerical model. Both phases are immiscible and incompressible fluids with equal density and viscosity. The relaxation follows the abrupt termination of a planar extensional flow, which, in turn, determines the droplet's initial shape. The relaxation of initially elongated regular viscous droplets has been studied in the last decades, giving rise to important contributions in areas such as microfluidics, food processing, and pharmaceuticals. However, to the best of our knowledge, studies of initially elongated magnetic responsive droplets under the influence of magnetic fields during the relaxation process have not been published yet. The present study focuses on how the magnetic field, together with the capillary relaxation, affects the breakup pattern of initially elongated ferrofluid droplets. The magnetic capillary number, which measures the ratio between magnetic stress and surface tension, the dimensionless rotational frequency of the magnetic field (zero for static field), the initial magnetic field direction, and the axis of rotation are the key parameters considered in the analysis. The full incompressible Navier-Stokes equations with capillary and magnetic source terms are solved using the classical projection method in a staggered grid, while the interface capturing problem is treated using a level-set method with conservative high-order time and space discretization. The validity of the method is confirmed by comparing the results for a regular droplet with previous numerical and experimental data. We present results comparing the relaxation pattern for different magnetic field rotational frequencies and directions of rotation. The simulation results reveal that the application of rotating magnetic fields can control the relaxation and breakup pattern of the droplets, altering the number and volume ratio of resulting daughter droplets by simply varying the rotational frequency. We also observed that rotating magnetic fields can induce breakup even when the droplet is initially elongated by the action of a magnetic field, eliminating the need for flow. These findings provide insights into new methods for controlling droplet breakup in microfluidic applications and magnetic emulsion formation.*

Keywords: *Droplet relaxation, Magnetic-induced breakup, Rotating field, Breakup control*

1. INTRODUCTION

The relaxation of viscous droplets is an important process regarding the stability of emulsion (Bentley and Leal, 1986). This problem was considered in the study of regular viscous droplets through experimental and numerical investigations (Ha and Leal, 2001; Biben *et al.*, 2003; Beaucourt *et al.*, 2007). The relaxation of non-regular polar droplets under the action of external fields, however, was not as widely studied. Only recently, Behera and Chakraborty (2022) investigated the effect of static uniform electric fields on the relaxation of initially elongated dielectric droplets, where it was observed that the breakup pattern can be altered.

Similarly, the relaxation dynamics of a ferrofluid droplet can be changed by magnetic fields. Ferrofluids are colloidal suspensions of magnetic particles in regular liquids, such as oil or water (Rosensweig, 2013). A droplet composed of a ferrofluid is magnetically responsive (see, for instance, (Afkhami *et al.*, 2010)). When in the presence of an external magnetic field, the magnetic stresses are induced at the droplet surface, which in turn elongates it in the direction of the external magnetic field. The effect of rotating magnetic fields on initially spherical ferrofluid droplets immersed in quiescent liquids has been studied in the last three decades (Bacri *et al.*, 1994; Erdmanis *et al.*, 2017; Zakinyan and Zakinyan, 2020). Using rotating fields, a variety of droplet shapes can be induced by varying the field intensity and the rotation frequency. Although some aspects of the behavior of ferrofluid droplets in rotating magnetic fields have already been established, there is no published analysis of the ferrofluid droplet relaxation under the action of rotating magnetic fields.

In this work, we study the relaxation process of ferrofluid droplets under the action of static and rotating magnetic fields. In Section 2. we describe the problem, the mathematical model, and the main nondimensional parameters. In Section 3. we expose the numerical settings. Then, in Section 4. we show the results of that investigation. Finally, in

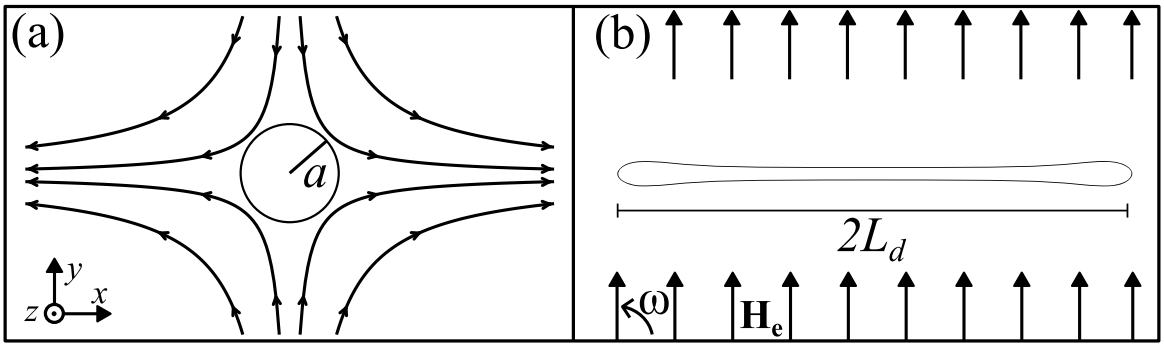

Figure 1. Problem sketch. (a) The droplet with an initial spherical shape of radius a is continuously stretched by the action of an external planar extensional flow. (b) The flow is abruptly stopped when the droplet reaches a size of $2L_d$ and the process of relaxation begins together with the application of an external uniform magnetic field $\mathbf{H_e} = \mathbf{H_0}$. In the case of a rotating magnetic field, it rotates with a rotational frequency ω. Both representations are in the xy-plane.

Section 5.we make our conclusions.

2. PROBLEM STATEMENT

The relaxation of initially elongated superparamagnetic ferrofluid droplets immersed in a nonmagnetizable viscous fluid is considered in this work. Both fluids have the same density, ρ, and viscosity, η. The interfacial tension coefficient between the phases is represented by σ. The ferrofluid has a constant magnetic susceptibility, χ. The numerical experiments consist of two steps: an elongation process followed by a relaxation process, as sketched in Fig. 1.

First [Fig. 1(a)], the droplet, initially spherical of radius a and located at the origin of the coordinate system, is submitted to an external planar extensional flow given by a velocity field far from the droplet, $\mathbf{u}_\infty$, equal to $\mathbf{u}_\infty = x\dot{\varepsilon}\hat{\mathbf{e}}_\mathbf{x} - y\dot{\varepsilon}\hat{\mathbf{e}}_\mathbf{y}$, where $\dot{\varepsilon}$ is the rate of extension. The flow-induced viscous forces tend to stretch the droplet in the x direction, while the capillary forces try to keep the droplet spherical. Provided the rate of extension has enough intensity, the droplet is continuously distorted and does not assume a steady state shape. Once the droplet reaches a length L_d in the x direction, the flow is stopped abruptly, and the relaxation process initiates.

The relaxation process here refers to the capillary relaxation in the absence of external flow. In this work, we consider the application of external magnetic fields throughout the system during the capillary relaxation, as sketched in Fig. 1(b). The applied external field, $\mathbf{H_e}$, is uniform in space and has a constant intensity in time. Static and rotating magnetic fields are explored. The rotating magnetic fields are defined by the initial direction, $\mathbf{H_0}$, the axis of rotation, $\mathbf{r}$, and the rotational frequency, ω. When the latter is positive, the external magnetic field rotates counterclockwise with respect to the axis of rotation. The evolution in time is given by

$$\mathbf{H_e}(t) = \mathbf{R}(\mathbf{r}, \omega, t) \cdot \mathbf{H_0} \tag{1}$$

where is the orthogonal rotation tensor defined as $\mathbf{R}(r, \omega, t) = \cos(2\pi\omega t)\mathbf{I} + \sin(2\pi\omega t)[\mathbf{r}]_x + [1 - \cos(2\pi\omega t)]\mathbf{rr}$, $\mathbf{I}$ is the identity tensor, and $[\mathbf{r}]_x$ is the cross product tensor of $\mathbf{r}$.

2.1 Mathematical equations

The ferrofluid droplet is considered superparamagnetic, meaning that when submitted to an external magnetic field, $\mathbf{H_0}$, the magnetization field inside the droplet, $\mathbf{M}$, is related to the local magnetic field $\mathbf{H}$ through the co-linear relation $\mathbf{M} = \chi\mathbf{H}$. In general, the magnetization follows Langevin dynamics marked by a linear region in low fields and a saturation region in high fields Rosensweig (2013). In our case, we assume a constant χ, provided that the magnetic field intensity is not high enough to surpass the linear regime, as did in other numerical studies on ferrofluid droplet dynamics. Since the continuous phase is nonmagnetizable, the magnetization in this region is null, and $\chi = 0$. We can define a piecewise constant function of space $\zeta(\mathbf{x}) = 1 + \chi$, which is $1 + \chi$ inside the droplet, and 1 outside.

Both fluids are electrically nonconducting materials. Therefore, the magnetic problem is treated using Maxwell's equations at the magnetostatic limit. They read

$$\nabla \times \mathbf{H} = \mathbf{0}, \text{ and } \nabla \cdot \mathbf{B} = 0, \tag{2}$$

where $\mathbf{H}$ is the magnetic field, and $\mathbf{B}$ is the magnetic induction field, related to $\mathbf{M}$ and $\mathbf{H}$ through $\mathbf{B} = \mu_0(\mathbf{H} + \mathbf{M})$, or, alternatively, through $\mathbf{B} = \mu_0\zeta(\mathbf{x})\mathbf{H}$. Due to the irrotationality, $\mathbf{H}$ is associated to the magnetic potential, ψ, through

$\nabla\psi = -\mathbf{H}$. Using this latter relation, the definition of $\mathbf{B}$ and its divergence-free nature, we have the following Poisson equation for the magnetic potential

$$\nabla \cdot (\zeta(\mathbf{x})\nabla\psi) = 0 \tag{3}$$

The motion of the system is governed by the incompressible Navier-Stokes equations with the addition of the capillary and magnetic force terms. The continuity equation reads

$$\nabla \cdot \mathbf{u} = 0, \tag{4}$$

and the momentum balance reads

$$\rho\left(\frac{\partial \mathbf{u}}{\partial t} + \mathbf{u}\cdot\nabla\mathbf{u}\right) = -\nabla p + \eta\nabla^2\mathbf{u} + \mathbf{F_c} + \mathbf{F_m}, \tag{5}$$

where $\mathbf{u}$ is the velocity field, p is the pressure field, and $\mathbf{F_c}$ and $\mathbf{F_m}$ are the capillary and magnetic forces per unit volume, respectively.

All the equations are solved over the whole domain. To address the difference in properties between the phases, we use the Level-Set method, better explained in Sec. 3.3. This method considers a signed distance function from the interface, ϕ, where negative values mean the region inside the droplet, positive values the region outside, and the zero level, $\phi = 0$, indicates the interface location. Using this variable and following the Young-Laplace condition, the capillary force term reads

$$\mathbf{F_c} = -\sigma\kappa\delta(\phi)|\nabla\phi|\hat{\mathbf{n}}, \tag{6}$$

where $\hat{\mathbf{n}}$ is the normal vector at the interface pointing outward of the droplet, σ is the interfacial tension coefficient, and κ is the local mean curvature of the interface. The magnetic force is the Kelvin force, $\mu_0\mathbf{M}\cdot\nabla\mathbf{H}$. In terms of $\zeta(\phi)$ and $\mathbf{H}$, it can be written as

$$\mathbf{F_m} = \mu_0(\zeta(\phi) - 1)\mathbf{H}\cdot\nabla\mathbf{H} \tag{7}$$

2.2 Boundary conditions

The boundaries in the z-direction are treated as periodic. For the magnetic potential equation, we set the von Neumann boundary conditions $\partial\psi/\partial n = -\mathbf{H_e}\cdot\mathbf{n}$ in all other boundaries, where $\mathbf{n}$ is the normal outward the domain boundaries. The velocity field far from the droplet $\mathbf{u}_\infty$ is set in all non-periodic boundaries. During the action of the planar extensional flow, the velocity field far from the droplet is that shown in Sec. 2. During the capillary relaxation, the velocity field far from the droplet $\mathbf{u}_\infty = \mathbf{0}$ is set at the domain boundaries. In both cases, the homogeneous von Neumann boundary condition is set for the pressure, $\partial p/\partial n = 0$.

2.3 Nondimensional equations

Two different types of flow are addressed in this problem. During the extension stage, the time scale of the problem is the inverse of the extension rate, $1/\dot{\varepsilon}$. During the capillary relaxation, the capillary time $\eta a/\sigma$ is the characteristic scale. We must set the remaining characteristic scales accordingly. In both cases, the length scale is the droplet radius, a, and the scale for the magnetic field is the applied magnetic field intensity, H_e. The magnetic potential is normalized by H_e/a. For the extension stage, we set $1/\dot{\varepsilon}$ for time, $\dot{\varepsilon}a$ for velocity, and $\rho\dot{\varepsilon}^2a^2$ for pressure. Using this scaling, the nondimensional momentum equation is given by

$$\frac{\partial \mathbf{u}}{\partial t} + \mathbf{u}\cdot\nabla\mathbf{u} = -\nabla p + \frac{1}{Re}\nabla^2\mathbf{u} - \frac{1}{ReCa}\kappa\delta(\phi)|\nabla\phi|\hat{\mathbf{n}} + \frac{Ca_{mag}}{ReCa}(\zeta(\phi) - 1)\mathbf{H}\cdot\nabla\mathbf{H} \tag{8}$$

where Re, Ca, and Ca_{mag} are the nondimensional groups for the extension stage, and the physical variables $\mathbf{u}$, p, κ, and $\mathbf{H}$ are already in their nondimensional form. The Reynolds number, Re, defined as $Re = \rho\dot{\gamma}a^2/\eta$, measures the importance of the inertia over the viscous forces. The capillary number, Ca, defined as $Ca = \eta\dot{\gamma}a/\sigma$, measures the ratio between the viscous and capillary forces. The magnetic capillary number, Ca_{mag}, defined as $Ca_{mag} = \mu_0 H_0^2 a/\sigma$,

measures the ratio between the magnetic and capillary forces. We assume the motion to be inertia-free, $Re \ll 1$, provided that the droplet is small enough.

For the relaxation stage, there is no more external flow, so the characteristic time scale is $\eta a/\sigma$. Using this time scale, we set σ/η for the velocity scale, and $\rho\sigma^2/\eta^2$ for the pressure scale. This scaling leads to the following nondimensional momentum equation, with the physical variables in its nondimensional forms:

$$\frac{\partial \mathbf{u}}{\partial t} + \mathbf{u}\cdot\nabla\mathbf{u} = -\nabla p + \frac{1}{Su}\nabla^2\mathbf{u} - \frac{1}{Su}\kappa\delta(\phi)|\nabla\phi|\hat{\mathbf{n}} + \frac{Ca_{mag}}{Su}(\zeta(\phi)-1)\mathbf{H}\cdot\nabla\mathbf{H} \tag{9}$$

where Su, and Ca_{mag} are the governing parameters. The nondimensional group Su, the Surutman number defined as $Su = \rho a\sigma/\eta^2$, measures the importance of the inertia over the capillary forces. As the Reynolds number, we have that $Su \ll 1$.

In both cases, the continuity equation and the magnetic potential equation have the same form as the dimensional ones, Eq. (4) and Eq. (3), respectively. The viscous terms in the momentum balance equations are slightly different if we consider a viscosity difference between the phases, as is the case in the validation case evaluated later. In this case, there is a viscosity ratio λ between the droplet shear viscosity, η_d, and the continuous phase shear viscosity, η, so that $\lambda = \eta_d/\eta$. In that case, the viscous term reads $(1/Re)\nabla\cdot[\eta_\varepsilon(\phi)(\nabla\boldsymbol{u} + \nabla\boldsymbol{u}^T)]$, where $\eta_\varepsilon(\phi)$ varies between η outside the droplet and $\lambda\eta$ inside the droplet.

3. COMPUTATIONAL SOLUTION

In this section, we describe the numerical model used to solve in space and time the equations Eq. (3), Eq. (4), and Eq. (8). The numerical model includes the projection method [Sec. 3.2] to solve the equations of motion, and the Level-Set method [Sec. 3.3] to solve the interface problem. The numerical model uses a finite difference scheme in a staggered grid (also called Marker-and-Cell grid) with scalars defined in the cell centers and vector components in their respective cell faces (Kim and Moin, 1985).

3.1 Magnetic potential

A Conjugated-Gradient method with multigrid preconditionning is used to solve the magnetic potential equation.

3.2 Projection method

The incompressible Navier-Stokes equations, including the momentum balance and continuity, are solved by using the projection method proposed in (Kim and Moin, 1985). The method consists in splitting the advancing in time into two steps. First, starting from the velocity $\mathbf{u}^n$ at the present time step, a tentative velocity field $\mathbf{u}^\star$ is obtained by ignoring the pressure term in Eq. (8). In this step, a semi-implicit Crank-Nicolson scheme is used, where the viscous term is treated semi-implicitly, and the convective and the body forces per unit volume, $\mathbf{F_c}$ and $\mathbf{F_m}$, are treated explicitly using a second-order Adams-Bashforth scheme. The first step reads

$$\frac{\mathbf{u}^\star - \mathbf{u}^n}{\Delta t} = -(\mathbf{u}\cdot\nabla\mathbf{u})^{n+1/2} + \frac{1}{2Re}\nabla^2(\mathbf{u}^n + \mathbf{u}^\star) + \frac{1}{ReCa}\mathbf{F_c}^{n+1/2} + \frac{Ca_{mag}}{ReCa}\mathbf{F_m}^{n+1/2}, \tag{10}$$

where Δt is the time step. The second step is obtained by comparing Eq. (10) to the discretized version of Eq. (8), and noting that the field in the pressure term is not the true pressure field, but an auxiliary pressure field, q. It reads

$$\frac{\mathbf{u}^{n+1} - \mathbf{u}^\star}{\Delta t} = -\nabla q^{n+1}. \tag{11}$$

Taking the divergence of Eq. (11) and imposing the incompressibility constraint, $\nabla\cdot\mathbf{u}^{n+1} = 0$, we find that the auxiliary pressure must satisfy the Poisson equation

$$\nabla^2 q^{n+1} = \frac{1}{\Delta t}\nabla\cdot\mathbf{u}^\star. \tag{12}$$

In summary, the projection method consists in solving the equation for the tentative velocity [Eq. (10)], finding the auxiliary pressure field [Eq. (12)], and then updating the true velocity field through Eq. (11). If required, the true pressure field can be computed from $p^{n+1} = q^{n+1} + (\Delta t/2Re)\nabla^2 q^{n+1}$. Note that, the projection method was explained for the case in which $\lambda = 1$. In the case of $\lambda \neq 1$, the viscous term is treated using a semi-implicit procedure proposed in the work of $Badalassi et\ al.$ (2003).

The boundary conditions for q are the same used for p, i.e., the homogeneous von Neumann condition. The boundary condition for $\mathbf{u}^\star$ is obtained by using Eq. (11), the boundary condition for $\mathbf{u}$, and the extrapolation $q^{n+1} = 2q^n - q^{n-1}$.

3.3 Level-Set method

The interface problem is treated with the well-established Level-Set method, which is already used in numerical studies of ferrofluid droplets (Zhu *et al.*, 2011; Cunha *et al.*, 2018, 2020; Abicalil *et al.*, 2021; Guilherme *et al.*, 2023). This method consists of evolving a signed distance function ϕ, in which the zero level corresponds to the interface between the phases, being the positive values referent to the matrix and the negative values to the droplet. The droplet is initialized as a sphere of radius a so that ϕ is easily distributed throughout the domain. The signed distance function is thus advected with the flow through the advection equation (Sussman *et al.*, 1994):

$$\frac{\partial \phi}{\partial t} + \mathbf{u} \cdot \nabla \phi = 0 \tag{13}$$

The interface can be then captured at any simulation time. The level-set permits a smooth transition of properties between the phases. A small value ϵ is defined to be this narrow band surrounding the interface in which the property varies from one phase to the other, and a smooth Heaviside function H_ϵ is applied (Sussman *et al.*, 1998):

$$H_\epsilon(\phi) = \begin{cases} 0, & \text{if } \phi < -\epsilon, \\ \frac{1}{2}\left[1 + \frac{\phi}{\epsilon} - \frac{1}{\pi}\sin \pi\phi/\epsilon\right], & \text{if } |\phi| \leq \epsilon, \\ 1, & \text{if } \phi > \epsilon \end{cases} \tag{14}$$

The corresponding delta function $\delta(\phi)$ is the derivative of H_ϵ with respect to ϕ. The interface thickness is generally chosen to be, as in this work, $\epsilon = 1.5h$ where h is the size of the grid cell. This smooth Heaviside is used for example to obtain a more spatially general smooth ϕ_f, replacing it by $\phi_{f-general}(\phi) = \phi_f[1 - H_\epsilon(\phi)]$. Although Eq. (13) accurately transports the level zero, i.e., interface, it deviates from the signed distance function along the iterations. Methods for reinitializing ϕ at each time step are implemented in this work, including volume constraints that guarantee the conservation of volume (Sussman and Fatemi, 1999). The conservative level-set approach of Sussman and Fatemi (1999) is used in our code. The reader is referred to Abicalil *et al.* (2021) for a more detailed explanation of the conservative level-set method used in this work including details of the reinitialization process.

3.4 Numerical settings

The ordinary spatial derivatives are treated using second-order finite differences schemes, with the exception of the advection terms of the momentum equation which uses a second-order non-oscillatory (ENO) scheme, and the advection term of the level-set equation, which uses a fifth-order weighted non-oscillatory (WENO) scheme (Jiang and Peng, 2000). Poisson's equations are discretized with second-order finite differences. A time step of $\Delta t = 3e - 3$ was used. The domain is of dimensions $20a$ x $10a$ x $7.5a$ for all cases and is discretized in 192 x 96 x 72 nodes.

4. RESULTS

All the results are for $Re = 0.01$, $Su = 0.01$, and $\chi = 1$, unless otherwise said. In all cases, the droplet is elongated until $L_d = 7.48$ with $Ca = 0.13$ before starting the relaxation process, unless otherwise said.

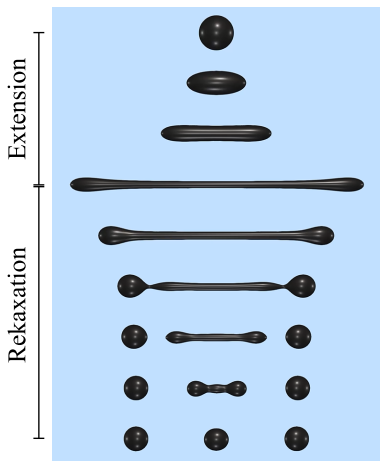

Figure 2. Extension and relaxation process with $Ca = 0.13$ and $L_d = 7.48$.

Figure 2 shows the extension stage and the relaxation process without the presence of external magnetic fields. During the extension, the droplet develops bulbous ends and necking regions. Once the relaxation starts, the bulbous ends become more pronounced and the droplet tips break off from the central part. While the central part tends to assume a spherical shape, new necking regions are created near the central droplet tips but are not enough to overcome the retraction of the droplet. As a result, the daughter droplets become stable and spherical shaped. The relaxation process in this case results in three daughter droplets of around the same volume.

To confirm the reliability of our numerical model, we compared the relaxation process and the final shape of the droplet for $\lambda = 0.2$ and $Ca = 0.159$ with the results of Beaucourt *et al.* (2007). The results are shown in Fig. 3. We can see a good agreement, which confirms the reliability of our model. It should be noted that earlier validations comparing steady shape results obtained in earlier works using the same numerical model already established the model's magnetic part (Abicalil *et al.*, 2021; Guilherme *et al.*, 2023).

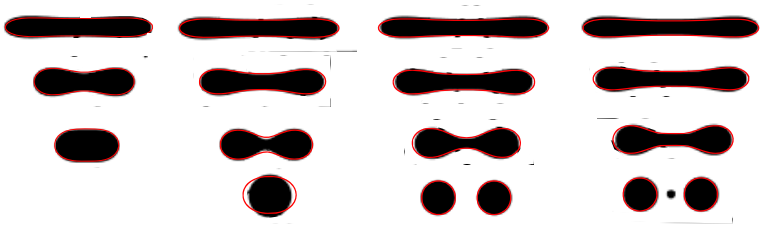

Figure 3. Comparison between the relaxations results for $\lambda = 0.2$, $Ca = 0.159$ and $L_d = 3.5, 3.8, 4.0$, and 4.2 (from left to right). Black droplets are the results of Beaucourt et al. (2007), and the red contours are the present results. In the case of $L_d = 3.8$, the last red contour is not spherical because the simulation was not complete.

The relaxation and breakup pattern of the elongated ferrofluid droplet can be changed by the application of magnetic fields. Figure 4 shows the relaxation process for a static magnetic field applied externally in the y-direction, and $Ca_{mag} = 25$. The initial condition for the relaxation process is the same as that of Fig. 2. In this case, the magnetic field pronounces even more the droplet tips due to the magnetic stresses that tend to elongate the droplet in the direction of the field. This changes the overall process. As a result, the breakup pattern is marked by the appearance of five daughter droplets. The way the magnetic field influences the relaxation process and the resulting pattern depends on the intensity of the magnetic field. Figure 5 shows that the transition between the three daughter droplets pattern with no magnetic field to five daughter droplets with $Ca_{mag} = 25$ occurs between $10 < Ca_{mag} < 15$.

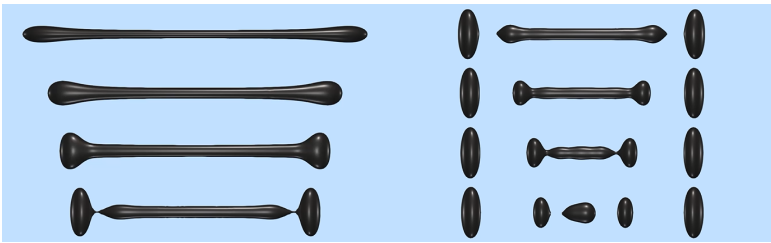

Figure 4. Relaxation process for $Ca = 0.13$ and $L_d = 7.48$ with the application of a static magnetic field with $Ca_{mag} = 25$.

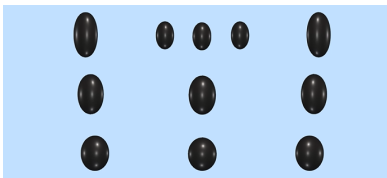

Figure 5. Relaxation process for $Ca = 0.13$ and $L_d = 7.48$ with the application of a static magnetic field. From top to bottom: $Ca_{mag} = 15$, 10, and 5.

Consider now the application of rotative magnetic fields. Figure 6 shows the relaxation process for a rotating magnetic field with the y-direction as the initial direction, a rotation axis pointing in the x direction, and $\omega = 0.5$. Ca_{mag} is kept equal to 25. The relaxation process is similar to that of the static field in the y-direction. In this case, the droplet breaks up into six daughter droplets.

The direction of rotation is also important. Figure 7 shows the relaxation process for a rotating magnetic field with the x-direction as the initial direction, a rotation axis pointing in the z direction, $\omega = 1$, and $Ca_{mag} = 25$. The droplet tips

Figure 6. Relaxation process for $Ca = 0.13$ and $L_d = 7.48$ with the application of a rotating magnetic field with $Ca_{mag} = 25$, $\omega = 0.5$ and the x-axis as the rotation axis.

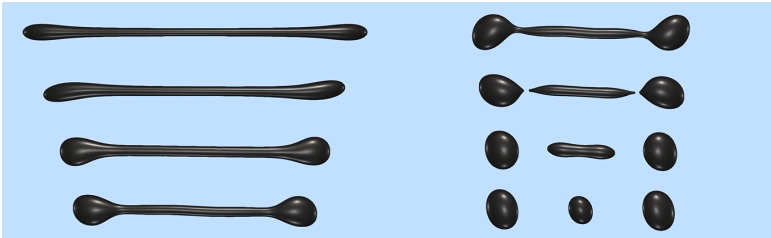

Figure 7. Relaxation process for $Ca = 0.13$ and $L_d = 7.48$ with the application of a rotating magnetic field with $Ca_{mag} = 25$, $\omega = 0.5$ and the z-axis as the rotation axis.

rotate in the xy plane, enhancing the cropping at the necking regions. In this case, the central droplet has a smaller volume compared to the case without magnetic field. The volume of the central droplet is 18.0% of the initial droplet volume. Increasing ω to 2 and 4, the central droplet volume portion decreases to 17.6%, and 15.4%, respectively. Decreasing ω to 0.5 and 0.25, the central droplet volume portion remains around the same, with a slight decrease, indicating a point of maximum at $\omega = 1$.

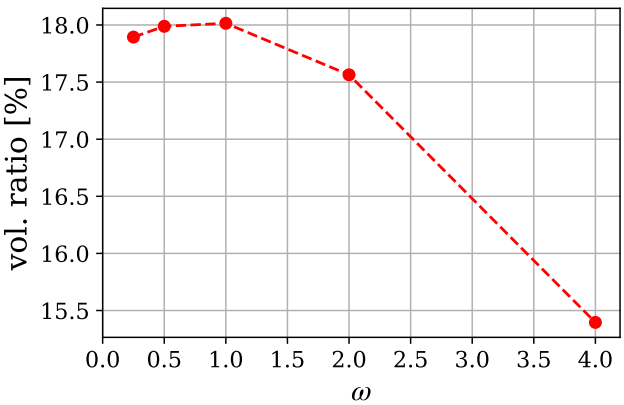

Figure 8. Ratio between the central daughter droplet volume and the initial droplet volume in percentages in the function of the rotational frequency ω. Results are for $L_d = 7.48$, $Ca = 0.13$, $Ca_{mag} = 25$, and the z-axis as the rotation axis.

We also observed the relaxation of a ferrofluid droplet (of $\chi = 2$) initially elongated with the action of a static uniform magnetic field at $Ca_{mag} = 35$. The intention behind this is to induce breakup without external flows. This possibility was confirmed as shown in Fig. 9. After elongating with a static magnetic field, the rotating field was started with $\omega = 0.035$. The droplet rotates at a different frequency compared to that of the magnetic field, inducing an S-shape. Then the droplet achieves a H-shape (red mark). At that moment, the magnetic field was stopped and the droplet broke up into two daughter droplets.

5. CONCLUSIONS

External magnetic fields can be used to control the relaxation and breakup process of ferrofluid droplets immersed in nonmagnetizable carrier fluids. The number of resulting daughter droplets is changed by changing the type, the direction of rotation of the applied magnetic field, and the magnetic field intensity. For a given direction of rotating magnetic field, the volume of the central droplet is dependent on the rotation frequency. The droplet breakup can be induced with rotating magnetic fields. It can serve as a new method of formation of emulsions without the need for external flows.

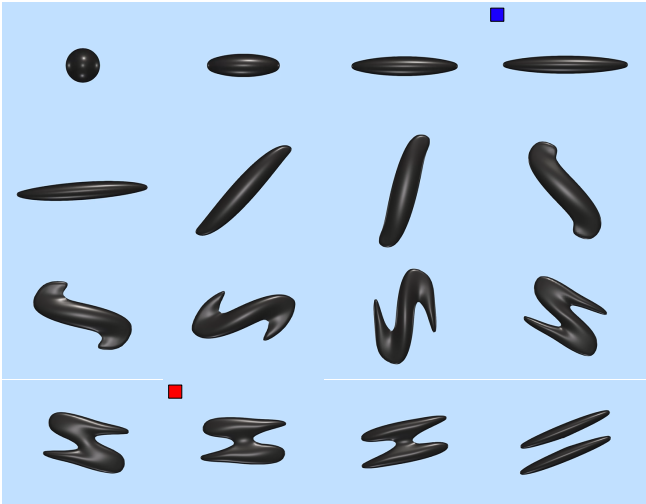

Figure 9. Magnetic-induced breakup. The droplet ($\chi = 2$) is initially stretched with a static uniform magnetic field with $Ca_{mag} = 35$ until the figure marked by a blue square ($L_d = 3.9$). Then the magnetic field rotates with $\omega = 0.035$ until the figure marked by a red square. From that, the magnetic field is kept static until breakup.

6. ACKNOWLEDGEMENTS

This research was supported by CNPq (Ministry of Science, Technology, and Innovation of Brazil) under grants 131422/2021-9 (A.L.G.), and 310631/2021-1 (T.F.O.); and by CAPES (Coordenação de Aperfeiçoamento de Pessoal de Nível Superior) under grant 88887.914649/2023-00 (A.L.G.).

7. REFERENCES

Abicalil, V.G.e., Abdo, R.F., da Cunha, L.H.P. and de Oliveira, T.F., 2021. "On the magnetization of dilute ferrofluid emulsions in shear flows". *Physics of Fluids*, Vol. 33, No. 5, p. 053313.

Afkhami, S.a., Tyler, A., Renardy, Y., Renardy, M., Pierre, T.S., Woodward, R. and Riffle, J.S., 2010. "Deformation of a hydrophobic ferrofluid droplet suspended in a viscous medium under uniform magnetic fields". *Journal of Fluid Mechanics*, Vol. 663, pp. 358–384.

Bacri, J.C., Cebers, A. and Perzynski, R., 1994. "Behavior of a magnetic fluid microdrop in a rotating magnetic field". *Physical review letters*, Vol. 72, No. 17, p. 2705.

Badalassi, V.E., Ceniceros, H.D. and Banerjee, S., 2003. "Computation of multiphase systems with phase field models". *Journal of computational physics*, Vol. 190, No. 2, pp. 371–397.

Beaucourt, J., Biben, T., Leyrat, A. and Verdier, C., 2007. "Modeling breakup and relaxation of newtonian droplets using the advected phase-field approach". *Physical Review E*, Vol. 75, No. 2, p. 021405.

Behera, N. and Chakraborty, S., 2022. "Electrically modulated relaxation dynamics of pre-stretched droplets post switched-off uniaxial extensional flow". *Soft Matter*, Vol. 18, No. 19, pp. 3678–3697.

Bentley, B. and Leal, L.G., 1986. "An experimental investigation of drop deformation and breakup in steady, two-dimensional linear flows". *Journal of Fluid Mechanics*, Vol. 167, pp. 241–283.

Biben, T., Misbah, C., Leyrat, A. and Verdier, C., 2003. "An advected-field approach to the dynamics of fluid interfaces". *Europhysics letters*, Vol. 63, No. 4, p. 623.

Cunha, L., Siqueira, I., Cunha, F. and Oliveira, T., 2020. "Effects of external magnetic fields on the rheology and magnetization of dilute emulsions of ferrofluid droplets in shear flows". *Physics of Fluids*, Vol. 32, No. 7, p. 073306.

Cunha, L.H., Siqueira, I.R., Oliveira, T.F. and Ceniceros, H.D., 2018. "Field-induced control of ferrofluid emulsion rheology and droplet break-up in shear flows". *Physics of Fluids*, Vol. 30, No. 12, p. 122110.

Erdmanis, J., Kitenbergs, G., Perzynski, R. and Cēbers, A., 2017. "Magnetic micro-droplet in rotating field: numerical simulation and comparison with experiment". *Journal of Fluid Mechanics*, Vol. 821, pp. 266–295.

Guilherme, A., Siqueira, I., Cunha, L., Thompson, R. and Oliveira, T., 2023. "Ferrofluid droplets in planar extensional flows: Droplet shape and magnetization reveal novel rheological signatures of ferrofluid emulsions". *Physical Review Fluids*, Vol. 8, No. 6, p. 063601.

Ha, J.W. and Leal, L.G., 2001. "An experimental study of drop deformation and breakup in extensional flow at high capillary number". *Physics of fluids*, Vol. 13, No. 6, pp. 1568–1576.

Jiang, G.S. and Peng, D., 2000. "Weighted eno schemes for hamilton–jacobi equations". *SIAM Journal on Scientific computing*, Vol. 21, No. 6, pp. 2126–2143.

Kim, J. and Moin, P., 1985. "Application of a fractional-step method to incompressible navier-stokes equations". *Journal of computational physics*, Vol. 59, No. 2, pp. 308–323.

Rosensweig, R.E., 2013. *Ferrohydrodynamics*. Courier Corporation.

Sussman, M. and Fatemi, E., 1999. "An efficient, interface-preserving level set redistancing algorithm and its application to interfacial incompressible fluid flow". *SIAM Journal on scientific computing*, Vol. 20, No. 4, pp. 1165–1191.

Sussman, M., Fatemi, E., Smereka, P. and Osher, S., 1998. "An improved level set method for incompressible two-phase flows". *Computers & Fluids*, Vol. 27, No. 5-6, pp. 663–680.

Sussman, M., Smereka, P. and Osher, S., 1994. "A level set approach for computing solutions to incompressible two-phase flow". *Journal of Computational physics*, Vol. 114, No. 1, pp. 146–159.

Zakinyan, A.R. and Zakinyan, A.A., 2020. "Rotating field induced torque on ferrofluid emulsion with deformable dispersed phase microdrops". *Sensors and Actuators A: Physical*, Vol. 314, p. 112347.

Zhu, G.P., Nguyen, N.T., Ramanujan, R.V. and Huang, X.Y., 2011. "Nonlinear deformation of a ferrofluid droplet in a uniform magnetic field". *Langmuir*, Vol. 27, No. 24, pp. 14834–14841.

8. RESPONSIBILITY NOTICE

The authors are solely responsible for the printed material included in this paper.